

# Modelling power-law spread of infectious diseases

Sebastian Meyer\*      Leonhard Held\*

Short-time human travel behaviour can be well described by a power law with respect to distance. We incorporate this information in space-time models for infectious disease surveillance data to better capture the dynamics of disease spread. Two previously established model classes are extended, which both decompose disease risk additively into endemic and epidemic components: a space-time point process model for individual point-referenced data, and a multivariate time series model for aggregated count data. In both frameworks, the power-law spread is embedded into the epidemic component and its decay parameter is estimated simultaneously with all other unknown parameters using (penalised) likelihood inference. The performance of the new approach is investigated by a re-analysis of individual cases of invasive meningococcal disease in Germany (2002–2008), and count data on influenza in 140 administrative districts of Southern Germany (2001–2008). In both applications, the power-law formulations substantially improve model fit and predictions. Implementation in the R package **surveillance** allows to apply the approach in other settings.

Key words: power law; distance decay function; infectious disease surveillance; stochastic epidemic modelling.

---

\*Division of Biostatistics, Institute of Social and Preventive Medicine, University of Zurich, Switzerland

## 1. Introduction

The surveillance of infectious diseases constitutes a key issue of public health and modelling their spread is basic to the prevention and control of epidemics. An important task is the timely detection of disease outbreaks, for which popular methods are the Farrington algorithm (Farrington et al., 1996; Noufaily et al., 2013) and cumulative sum (CUSUM) likelihood ratio detectors inspired from statistical process control (Höhle et al., 2009). As opposed to such prospective surveillance, retrospective surveillance is concerned with explaining the spread of an epidemic through statistical modelling, thereby assessing the role of environmental and socio-demographic factors or contact networks in shaping the evolution of an epidemic. The spatio-temporal data for such modelling primarily originates from routine public health surveillance of the occurrence of infectious diseases, and is ideally accompanied by additional data which carry information on influential factors to be accounted for. Surveillance data are available in different spatio-temporal resolutions each type requiring an appropriate model framework.

This paper covers both a spatio-temporal point process model for individual-level data (proposed by Meyer et al., 2012, motivated by the work of Höhle, 2009), and a multivariate time-series model for aggregated count data (established by Held and Paul, 2012, and earlier work). Although these two models are designed for different types of spatio-temporal surveillance data, they are both inspired by the work of Held et al. (2005) decomposing disease risk additively into “endemic” and “epidemic” components. The endemic component captures exogeneous factors such as population, socio-demographic variables, long-term trends and seasonality, climate, or concurrent counts of related diseases in humans or animals (all varying in time and/or space). Explicit dependence between observed cases, i.e., infectiousness, is then introduced through epidemic components driven by the observed past. To describe disease spread in space, both models account for spatial interaction between units or individuals, respectively, and this is where this paper comes into play.

Up to now, spatial dispersal has been incorporated rather crudely in both models. For instance, the point process model used a Gaussian kernel to

capture spatial interaction, and the multivariate time-series model restricted epidemic spread from time  $t$  to  $t + 1$  to adjacent regions. However, a simple but exceedingly well-fitting form of dispersal can be motivated by the findings of [Brockmann et al. \(2006\)](#): they inferred from the dispersal of bank notes in the United States that short-time human travel can be well described by a decreasing power law as a function of distance  $x$ , i.e.  $f(x) \propto x^{-d}$  with positive decay parameter  $d$ . An important characteristic of this power law is its slow convergence to zero (“heavy tail”), which in our application enables occasional long-range transmissions of infectious agents apart from the principal mass of short-range infections. In the words of [Brockmann et al. \(2006\)](#), the power-law feature of short-time human travel provides a “starting point for the development of a new class of models for the spread of human infectious diseases”.

Power laws are well-known from the work by [Pareto \(1896\)](#) for the distribution of income and [Zipf \(1949\)](#) for city sizes and word frequencies in texts. They describe the distribution of earthquake magnitudes ([Gutenberg and Richter, 1944](#)) and many other natural phenomena (see [Newman, 2005](#); [Pinto et al., 2012](#), for a review of power laws). [Liljeros et al. \(2001\)](#) reported on a power-law distribution of the number of sexual partners, and [Albert and Barabási \(2002\)](#) review recent advances in network theory including scale-free networks where the number of edges is distributed according to a power law. Interestingly, a power law was also used as the distance decay function in geographic profiling for serial violent crime investigation ([Rossmo, 2000](#)) as well as in an application of this technique to infectious disease control ([Le Comber et al., 2011](#)). Examples of power-law transmission kernels to model the spatial dynamics of infectious diseases can be found in plant epidemiology ([Gibson, 1997](#); [Soubeyrand et al., 2008](#)) and in models for the 2001 UK foot-and-mouth disease epidemic ([Chis Ster and Ferguson, 2007](#)). Recently, [Geilhufe et al. \(2013\)](#) found that using (fixed) power-law weights between regions performed better than real traffic data in predicting influenza counts in Northern Norway. However, in both models for spatio-temporal surveillance data presented in the following sections, the decay parameter  $d$  will be estimated simultaneously with all other unknown parameters.

This paper is organised as follows: In Sections 2 and 3, respectively, the two model frameworks are reviewed and extended with a power-law formulation for the spatial interaction of units. In Section 4, surveillance data on invasive meningococcal disease (IMD) and influenza are re-analysed using power laws, which are evaluated against previously used models for these data. We close with some discussion in Section 5 and a software overview in Section 6.

## 2. Individual-level model

### 2.1. Introduction

The spatio-temporal point process model proposed by Meyer et al. (2012) is designed for individual case report data to describe the occurrence of infections (“events”) and their potential to trigger secondary cases. Formally, the model characterises a spatio-temporal point process in a region  $\mathbf{W}$  observed during a period  $(0, T]$  through the conditional intensity function

$$\lambda(t, \mathbf{s}) = v_{[t][\mathbf{s}]} \rho_{[t][\mathbf{s}]} + \sum_{j:t_j < t} \eta_j \cdot g(t - t_j) \cdot f(\|\mathbf{s} - \mathbf{s}_j\|). \quad (1)$$

Related models are the purely temporal, “self-exciting” process proposed by Hawkes (1971), the spatio-temporal epidemic-type aftershock-sequences (ETAS) model from earthquake research (Ogata, 1998), the spatio-temporal point process models by Diggle (2007) and an additive-multiplicative point process model for continuous-time discrete-space surveillance data proposed by Höhle (2009).

The first, endemic component in model (1) consists of a log-linear predictor  $\log(v_{[t][\mathbf{s}]}) = \beta_0 + \boldsymbol{\beta}^\top \mathbf{z}_{[t][\mathbf{s}]}$  proportional to an offset  $\rho_{[t][\mathbf{s}]}$ , typically the population density. Both, the offset and the exogenous covariates are given piecewise constant on a spatio-temporal grid (e.g. week  $\times$  district), hence the notation  $[t][\mathbf{s}]$  for the period which contains  $t$  in the region covering  $\mathbf{s}$ . In the IMD application in Section 4.1 for example,  $\mathbf{z}_{[t][\mathbf{s}]} = ([t], \sin(\omega \cdot [t]), \cos(\omega \cdot [t]))^\top$  incorporates a time trend with one sinusoidal wave of frequency  $\omega = 2\pi/365$ .

A purely endemic, piecewise constant intensity model without the observation-driven epidemic component is equivalent to a Poisson regression model for the

aggregated number of cases on the chosen spatio-temporal grid. However, with an epidemic component the intensity process depends on previously infected individuals and becomes “self-exciting”. Specifically, the epidemic force of infection at  $(t, \mathbf{s})$  results as the superposition of the infection pressures caused by each previously infected individual  $j$ . The individual infection pressure is weighted by the log-linear predictor  $\log(\eta_j) = \gamma_0 + \boldsymbol{\gamma}^\top \mathbf{m}_j$ , which models the effect of individual/infection-specific characteristics  $\mathbf{m}_j$  such as the age of the infective. Regional-level covariates could also be included in  $\mathbf{m}_j$ , e.g. to model ecological effects on infectivity. Note, however, since the epidemic is modelled through a point process, the susceptible “population” consists of the continuous observation region  $\mathbf{W} \subset \mathbb{R}^2$  and is thus infinite. Consequently, the model cannot include information on susceptibles, nor an autoregressive term as in time-series models.

Decreasing infection pressure of  $j$  over space and time is described by  $f(x)$  and  $g(t)$ , parametric functions of the spatial distance  $x$  and of the elapsed time  $t$  since  $j$  became infectious, respectively. The spatial interaction could also be described more generally by a non-isotropic function  $f_{2D}(\mathbf{s})$  of the vector  $\mathbf{s}$  to the host, e.g. to incorporate the dominant wind direction in vector-borne diseases. However, in our application,  $f$  essentially reflects people’s movements and we assume that  $f_{2D}(\mathbf{s}) = f(\|\mathbf{s}\|)$  only depends on the distance to the host. For instance, [Meyer et al. \(2012\)](#) used an isotropic Gaussian kernel

$$f(x) = \exp\left(-\frac{x^2}{2\sigma^2}\right). \quad (2)$$

In what follows, we propose an alternative specification of  $f(x)$ , which allows for occasional long-range transmissions of infections: a power law. As in [Meyer et al. \(2012\)](#),  $g(t) = \mathbb{1}_{[0,30]}(t)$  is used, i.e., constant infectivity over time until 30 days after infection when infectivity vanishes to zero.

## 2.2. Power-law extension

The basic power law  $f(x) = x^{-d}$ ,  $d > 0$ , is not a suitable choice for the distance decay of infectivity, since  $f_{2D}(\mathbf{s}) = f(\|\mathbf{s}\|)$  would not be integrable over a

domain including the origin. For  $x \geq \sigma > 0$ ,  $x^{-d}$  is the kernel of a Pareto density, but a shifted version for the domain  $\mathbb{R}_0^+$ , known as Pareto type II and sometimes named after [Lomax \(1954\)](#) has the density kernel

$$f(x) = (x + \sigma)^{-d} \quad (3)$$

(see Fig. 1a). Note that there is no need for  $f$  to be normalised to a density. Actually, the spatial interaction function  $f$  is more closely related to correlation functions known from stationary random field models for geostatistical data ([Stein, 1999](#)). By reparametrising (3) as  $f(x)/\sigma^{-d} = (1 + x/\sigma)^{-d}$  one obtains a member of the Cauchy family introduced by [Gneiting and Schlather \(2004\)](#), which provides asymptotic power-law correlation as  $x \rightarrow \infty$  with “long-memory parameter”  $d$  and smoothness parameter set to 1.

For short-range travel within 10 km, [Brockmann et al. \(2006\)](#) found a uniform distribution instead of power-law behaviour, which suggests an alternative formulation with a “lagged” power law:

$$f_L(x) = \begin{cases} 1 & \text{for } x \leq \sigma, \\ \left(\frac{x}{\sigma}\right)^{-d} & \text{otherwise.} \end{cases} \quad (4)$$

Now dispersal is constant up to the short-range threshold  $\sigma > 0$ , followed by a power-law decay for larger distances (see Fig. 1b). A similar kernel was used by [Deardon et al. \(2010\)](#), therein called “geometric”) for the 2001 UK foot-and-mouth disease epidemic, additionally limiting spatial interaction to a pre-specified upper-bound distance.

### 2.3. Inference

In both power-law formulations, the parameters  $d$  and  $\sigma$  can be estimated via numerical maximisation of the full (log-)likelihood. Note that they are estimated on the log-scale to avoid constrained optimisation. We use a quasi-Newton algorithm (cf. Section 6) incorporating the analytical gradient and Hessian for efficient optimisation. The required first partial derivatives of  $f$  or  $f_L$  with respect to the log-parameters are listed in Appendix A.1.

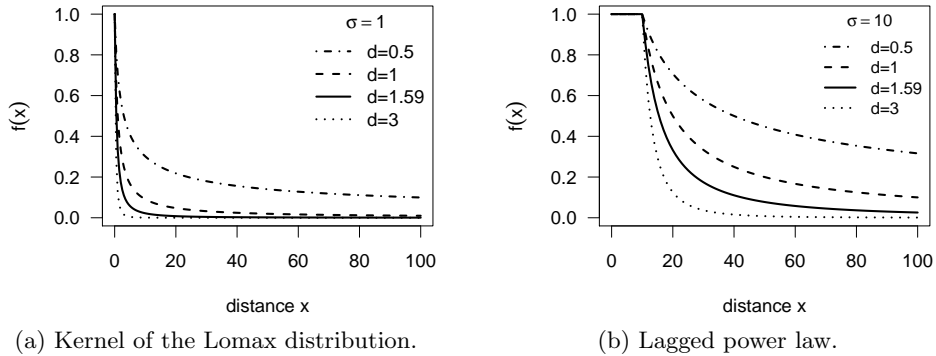


Figure 1: Power-law kernels for various choices of the decay parameter  $d > 0$ .

The point process likelihood incorporates the integral of  $f_{2D}(\mathbf{s})$  over shifted versions of the observation region  $\mathbf{W}$ , which is represented by polygons. The same is true for the score function and approximate Fisher information with  $f_{2D}$  replaced by its partial derivatives. This requires a method of numerical integration such as the two-dimensional midpoint rule, which was used by Meyer et al. (2012) for the Gaussian kernel. Here, we use the more sophisticated approach of product Gauss cubature over polygons proposed by Sommariva and Vianello (2007). This cubature rule is based on Green’s theorem, which relates the double integral over the polygon to a line integral along the polygon boundary. Numerical efficiency could be improved further by taking analytical advantage of the isotropy of  $f_{2D}$  in our specific case. Regardless of any sophisticated cubature rule, this is the part that makes model fitting cumbersome, since it introduces numerical errors which have to be controlled such that they do not corrupt numerical likelihood maximisation, and it increases computational cost by several orders of magnitude. For instance, in our IMD application in Section 4.1 a single likelihood evaluation would only take 0.4 seconds if we used a constant spatial dispersal  $f(x) \equiv 1$ , where the integral does not depend on parameters being optimised and simply equals the area of the polygonal domain. For the Gaussian kernel, a single evaluation takes about 6 seconds, and the power law takes about 100 seconds since its heavy tail requires more evaluation nodes for the numerical integration to be accurate enough.

### 3. Count data model

#### 3.1. Introduction

The multivariate time-series model established by [Held and Paul \(2012\)](#) (see also [Paul and Held, 2011](#); [Paul et al., 2008](#); [Held et al., 2005](#)) is designed for spatially and temporally aggregated surveillance data, i.e., disease counts  $Y_{it}$  in regions  $i = 1, \dots, I$  and periods  $t = 1, \dots, T$ . Formally, the counts  $Y_{it}$  are assumed to follow a negative binomial distribution

$$Y_{it} | \mathbf{Y}_{\cdot, t-1} \sim \text{NegBin}(\mu_{it}, \psi) \quad i = 1, \dots, I, t = 1, \dots, T$$

with additively decomposed mean

$$\mu_{it} = \nu_{it} e_{it} + \lambda_{it} Y_{i, t-1} + \phi_{it} \sum_{j \neq i} w_{ji} Y_{j, t-1}, \quad (5)$$

and overdispersion parameter  $\psi$  such that the conditional variance of  $Y_{it}$  is  $\mu_{it}(1 + \psi\mu_{it})$ . The Poisson distribution results as a special case if  $\psi = 0$ . In Eq. (5), the first component represents the endemic component similar to the point process model (1). The endemic mean is proportional to an offset of known expected counts  $e_{it}$  typically reflecting the population at risk. The other two components are observation-driven epidemic components: The second component models an autoregression on the number of cases at the previous time point, whereas the third, “spatio-temporal” component captures transmission from other units. Note that without these epidemic components, the model would reduce to a negative binomial regression model for independent observations.

Each of the parameters  $\nu_{it}$ ,  $\lambda_{it}$ , and  $\phi_{it}$  is a log-linear predictor of the form

$$\log(\cdot_{it}) = \alpha^{(\cdot)} + b_i^{(\cdot)} + \boldsymbol{\beta}^{(\cdot)\top} \mathbf{z}_{it}^{(\cdot)}$$

(where “ $\cdot$ ” is one of  $\nu$ ,  $\lambda$ ,  $\phi$ ), containing fixed and region-specific intercepts as well as effects of exogenous covariates  $\mathbf{z}_{it}^{(\cdot)}$  including time effects. For example,



in the influenza application in Section 4.2,  $\mathbf{z}_{it}^{(v)} = (t, \boldsymbol{\zeta}_S^\top)^\top$  with

$$\boldsymbol{\zeta}_S = (\sin(1 \cdot \omega t), \cos(1 \cdot \omega t), \dots, \sin(S \cdot \omega t), \cos(S \cdot \omega t))^\top$$

describes an endemic time trend with a superposition of  $S$  harmonic waves of fundamental frequency  $\omega = 2\pi/52$  (Held and Paul, 2012). The random intercepts  $\mathbf{b}_i := (b_i^{(\lambda)}, b_i^{(\phi)}, b_i^{(v)})^\top$  account for heterogeneity between regions, and are assumed independent and identically distributed following  $N_3(\mathbf{0}; \boldsymbol{\Sigma})$ . Accounting for correlation of random intercepts across regions is possible by adopting a conditional autoregressive (CAR) model (Paul and Held, 2011).

The weights  $w_{ji}$  of the spatio-temporal component in (5) describe the strength of transmission from region  $j$  to region  $i$ , collected into a  $I \times I$  weight matrix  $(w_{ji})$ .<sup>1</sup> In contrast to the individual-level model, all of the  $Y_{j,t-1}$  cases of the neighbour  $j$  by aggregation contribute with the same weight  $w_{ji}$  to infections in region  $i$ . In previous work, these weights were assumed to be known and restricted to first-order neighbours:

$$w_{ji} = \begin{cases} 1/n_j & \text{for } i \sim j, \\ 0 & \text{otherwise,} \end{cases} \quad (6)$$

where the symbol “ $\sim$ ” denotes “is adjacent to” and  $n_j$  is the number of direct (first-order) neighbours of region  $j$ . This is a normalised version of the “raw” adjacency indicator matrix  $\mathbf{A} = (\mathbb{1}(i \sim j))_{j,i=1,\dots,I}$ , which is binary and symmetric. The idea behind normalisation is that each region  $j$  distributes its cases uniformly to its  $n_j$  neighbours (Paul et al., 2008). Accordingly, the weight matrix is normalised to proportions such that all rows sum to 1. A simple alternative weight matrix considering only first-order neighbours would result from the definition  $w_{ji} = 1/n_i$  for  $i \sim j$  (i.e. columns sum to 1), meaning that the number of cases in a region  $i$  at time  $t$  is promoted by the mean of the counts from neighbouring regions at time  $t - 1$ . However, the first definition seems more natural in the framework of branching processes, where the point of view is from the infective source. Furthermore, the factor  $1/n_i$  would be confounded

---

<sup>1</sup>Note that  $j$  is the row index of the weight matrix.

with the region-specific intercepts  $b_i^{(\phi)}$ .

In either case, with the above weight matrix, the epidemic can only spread to first-order neighbours during the period  $t \rightarrow t + 1$ , except for independently imported cases via the endemic component. This seems not appropriate regarding the ability of humans to travel further. If movement network data are available, the weight matrix could instead be based on the connectivity between regions (symmetric or even asymmetric), which was investigated by [Schrödle et al. \(2012\)](#) for the spread of Coxiellosis in Swiss cows, and [Geilhufe et al. \(2013\)](#) for the spread of influenza in Northern Norway. In what follows, we propose a parametric generalisation of the neighbourhood weights, which is suitable in the absence of network data: a power law.

### 3.2. Power-law extension

To implement the power-law principle in the network of geographical regions, we first need to define a distance measure on which the power law acts. There are two natural choices: Euclidean distance between the regions' centroid coordinates, and the order of neighbourhood between regions. The first one conforms to a continuous power law whereas the second one is discrete. However, using centroid coordinates interferes with the area and shape of the regions. Specifically, a tiny region adjacent to region  $i$  would be attributed a stronger link to  $i$  than a large region with centroid further apart, even if it shares much more of region  $i$ 's border than the tiny region does. Using the length of common border as a measure of coupling between regions would only cover adjacent regions. We thus opt for the discrete measure of neighbourhood order.

Formally, a region  $j$  is a  $k$ th-order neighbour of another region  $i$ , denoted  $o_{ji} = o_{ij} = k$ , if it is adjacent to a  $(k - 1)$ th-order neighbour of  $i$  and if it is not itself a neighbour of order  $k - 1$  of region  $i$ . In other words, two regions are  $k$ th-order neighbours, if the shortest route between them has  $k$  steps across distinct regions. The network of regions thus features a symmetric,  $I \times I$ , integer matrix of neighbourhood orders with zeroes on the diagonal by convention.

Given this discrete distance measure, we generalise the previously used first-order weight matrix to higher-order neighbours assuming a power law with

decay parameter  $d > 0$ :

$$w_{ji} = o_{ji}^{-d} \quad (7)$$

for  $j \neq i$ , and  $w_{jj} = 0$ . This may also be recognised as the kernel of the [Zipf \(1949\)](#) probability distribution. The raw power-law weights (7) can be normalised to

$$w_{ji} = \frac{o_{ji}^{-d}}{\sum_{k=1}^I o_{jk}^{-d}} \quad (8)$$

such that  $\sum_{k=1}^I w_{jk} = 1$  for all rows  $j$  of the weight matrix. The higher the decay parameter  $d$ , the less important are higher-order neighbours with  $d \rightarrow \infty$  corresponding to the previously used first-order dependency, and  $d = 0$  assigning equal weight to *all* other regions.

### 3.3. Inference

The incorporation of a parametric weight structure further increases the dimension of the likelihood. However, supplied with the corresponding score function and (observed) Fisher information matrix, estimation of  $d$  within the penalised likelihood framework established by [Paul and Held \(2011\)](#) is still possible (cf. [Appendix A.2](#)).

Classical model choice criteria such as Akaike’s Information Criterion (AIC) are generally not suitable for models with random effects. Therefore, performance of the power-law models and the previous first-order formulations is compared based on the assessment of one-step-ahead forecasts with strictly proper scoring rules: the logarithmic score (logS) and the ranked probability score (RPS) advocated by [Czado et al. \(2009\)](#) for count data.

$$\begin{aligned} \log S(P, y) &= -\log P(Y = y) \\ \text{RPS}(P, y) &= \sum_{k=0}^{\infty} [P(Y \leq k) - \mathbb{1}(y \leq k)]^2 \end{aligned}$$

Note that the infinite sum in the RPS can be approximated by truncation at some large  $k$  in a way such that a pre-specified absolute approximation error is maintained ([Wei and Held, 2013](#)). These scores evaluate the discrepancy

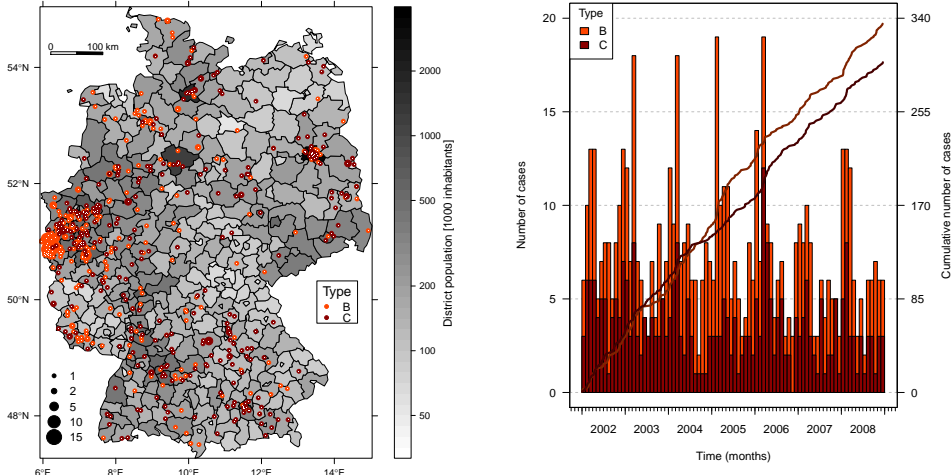
between the predictive distribution  $P$  from a fitted model and the later observed value  $y$ . Thus, lower scores correspond to better predictions. Such scoring rules have already been used for previous analyses of the influenza surveillance data (Held and Paul, 2012). Along these lines, we compute a set of one-week-ahead predictions and associated scores and then assess statistical significance of the difference in mean scores using a Monte-Carlo permutation test for paired data.

## 4. Applications

We now apply the power-law formulations of both model frameworks to previously analysed surveillance data and investigate potential improvements with respect to predictive performance. In Section 4.1, 635 individual case reports of IMD caused by the two most common bacterial finetypes of meningococci in Germany from 2002 to 2008 (see Meyer et al., 2012, and Fig. 2) are analysed with the point process model (1). In Section 4.2, the multivariate time-series model (5) is applied to weekly numbers of reported cases of influenza in the 140 administrative districts of the federal states Bayern and Baden-Württemberg in Southern Germany from 2001 to 2008 (see Held and Paul, 2012, and Fig. 4). In Section 4.3, we evaluate a simulation-based long-term forecast of the 2008 influenza wave. Space-time animations of both surveillance data sets are provided in the web-based Supplement A.

### 4.1. Cases of invasive meningococcal disease in Germany (2002–2008)

In the original analysis of the IMD data (Meyer et al., 2012), comprehensive AIC-based model selection yielded a linear time trend, a sinusoidal time-of-year effect ( $S = 1$ ), and no effect of the concurrent or lagged number of local influenza cases in the endemic component. The epidemic component included an effect of the meningococcal finetype (C:P1.5,2:F3-3 being less infectious than B:P1.7-2,4:F1-5, abbreviated by C and B in the following), a small age effect (3-18 year old patients tending to be more infectious), and supported an isotropic Gaussian spatial interaction function  $f$  compared to homogeneous



(a) Spatial point pattern with dot size proportional to the number of cases at the respective location (postcode level). (b) Monthly aggregated time series and evolution of the cumulative number of cases (original resolution: date of specimen sampling).

Figure 2: Distribution of the 635 IMD cases in Germany, 2002-2008, caused by the two most common meningococcal finetypes B:P1.7-2,4:F1-5 (335 cases) and C:P1.5,2:F3-3 (300 cases), as reported to and typed by the German Reference Centre for Meningococci. One case has been excluded due to missing age information.

spatial spread ( $f(x) \equiv 1$ ). In this paper, we replace the Gaussian kernel in the selected model by the proposed power-law distance decay (3) to investigate if it better captures the spatio-temporal clustering of cases.

Note that the distinction between two finetypes in this application actually corresponds to a marked version of the point process model (1). It is described by an intensity function  $\lambda(t, \mathbf{s}, \kappa)$ , where the sum in (1) is restricted to previously infected individuals of one specific bacterial finetype  $\kappa$ , since we assume that infections of different finetypes are not associated via transmission (Meyer et al., 2012). For convenience, we kept notation simple and comparable to the multivariate time-series model of Section 3.

Prior to fitting point process models to the IMD data, the interval-censored nature of the data due to a restricted resolution in space and time has to be taken into account: we only observed dates and residence postcodes of the

cases, and the model assumes that infections happened within the given region. This makes the data interval-censored yielding tied observations. However, ties are not compatible with our (continuous-time, continuous-space) point process model since observing two events at the exact same time point or location has zero probability. In the original analyses with a Gaussian kernel  $f$ , events were untied in time by subtracting a  $U(0,1)$ -distributed random number from all observed time points (Meyer et al., 2012), i.e., random sampling within each day, which is also the preferred method used by Diggle et al. (2010). To identify the two-parameter power law  $(x + \sigma)^{-d}$ , it was additionally necessary to break ties in space since otherwise  $\log \sigma$  diverged to  $-\infty$  yielding a pole at  $x = 0$ . A possible solution is to shift all locations randomly in space within their round-off intervals similar to the tie-breaking in time. In the absence of a shapefile of the postcode regions, we shifted locations by a vector uniformly drawn from the disc with radius  $\epsilon/2$ , where  $\epsilon$  was chosen as the minimum observed spatial separation of distinct points, here  $\epsilon = 1.17\text{km}$ . Accordingly, a sensitivity analysis was conducted by applying the random tie-breaking in time and space 30 times and fitting the models to all resulting datasets.

Figure 3a displays the estimated spatial interaction functions together with confidence intervals and estimates from the sensitivity analyses. The power-law kernel puts much more weight on localized transmissions with an initially faster distance decay of infectivity. Furthermore, it features a heavier tail than the Gaussian kernel, which facilitates the geographical spread of IMD by occasional long-range transmissions. Maps of the accumulated epidemic intensity in Supplement A visualise the impact of the modified kernel on the model. AIC clearly prefers the Lomax kernel against the Gaussian kernel ( $\Delta\text{AIC} = -28$ ). The estimated lagged version of the power law (4) displayed in Fig. 3b has a decay of  $\hat{d} = 1.69$  (95% CI: 1.52 to 1.88) and a uniform short-range dispersal radius of  $\hat{\sigma} = 0.40$  (95% CI: 0.18 to 0.86) kilometres. However, such a small  $\sigma$  is not interpretable since it is not covered by the spatial resolution of the data. This can also be seen from the 30 highly dispersed estimates obtained by sensitivity analysis. Moreover, the lagged power law has a higher AIC value than the Lomax kernel ( $\Delta\text{AIC} = 7$ ). We therefore do not further consider the lagged version for the IMD data.

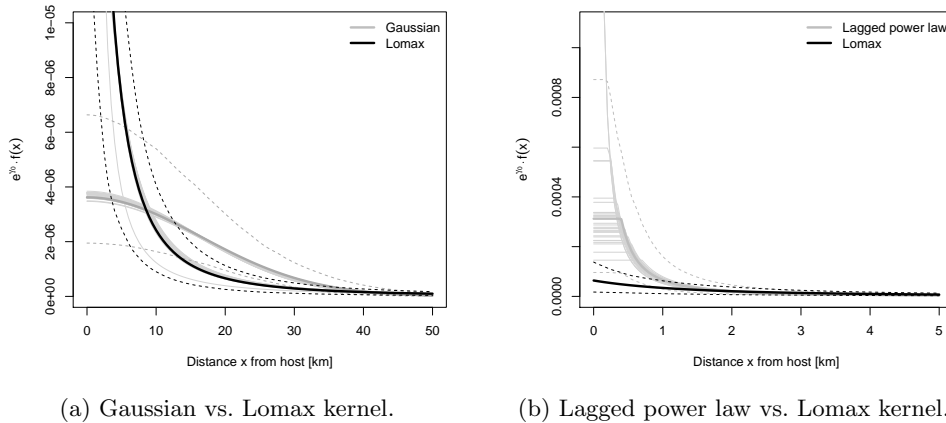


Figure 3: Estimated spatial interaction functions together with 95% bootstrap confidence intervals (dashed lines), i.e., the pointwise 2.5% and 97.5% quantiles of the functions evaluated for 999 samples from the asymptotic multivariate normal distribution of the affected parameters. The light grey lines are estimates obtained from repeated random tie-breaking as a means of sensitivity analysis.

For the Gaussian and Lomax model, sensitivity analysis of the random tie-breaking procedure in space and time generally confirmed the results. One replicate for the Lomax model yielded a slightly different shape of the power law, which is due to closely located points after random tie-breaking. Such an artifact would have been avoided if we had used constrained sampling in that the randomly shifted points obey a minimum separation of say 0.1 km.

Parameters estimates and confidence intervals for the Gaussian and Lomax models are presented in Table 2b. The parameters of the endemic component characterising time trend and seasonality were not affected by the change of the shape of the spatial interaction, and also the epidemic coefficients of finetype and age group do not differ much between the models retaining their signs and orders of magnitude.

An important quantity in epidemic modelling is the expected number  $R$  of offspring (secondary infections) each case generates. This reproduction number can be derived from the fitted models for each event by integrating its triggering function  $\eta;g(t)f(x)$  over space and time. Type-specific estimates of  $R$  are then obtained by averaging over the individual estimates by finetype. Table 3b

Table 1: Parameter estimates and 95% Wald confidence intervals for the Gaussian and the power-law model. Results for the Gaussian kernel are slightly different from those reported by Meyer et al. (2012) due to improved numerical integration.

	Estimate	95% CI		Estimate	95% CI
$\beta_0$	-20.53	-20.62 to -20.44	$\beta_0$	-20.58	-20.68 to -20.47
$\beta_{\text{trend}}$	-0.05	-0.09 to -0.00	$\beta_{\text{trend}}$	-0.04	-0.09 to 0.00
$\beta_{\text{sin}}$	0.26	0.14 to 0.39	$\beta_{\text{sin}}$	0.26	0.12 to 0.39
$\beta_{\text{cos}}$	0.26	0.14 to 0.39	$\beta_{\text{cos}}$	0.27	0.14 to 0.40
$\gamma_0$	-12.53	-13.15 to -11.91	$\gamma_0$	-7.01	-9.47 to -4.54
$\gamma_C$	-0.91	-1.44 to -0.39	$\gamma_C$	-0.79	-1.31 to -0.28
$\gamma_{3-18}$	0.67	0.04 to 1.31	$\gamma_{3-18}$	0.80	0.12 to 1.48
$\gamma_{\geq 19}$	-0.29	-1.19 to 0.61	$\gamma_{\geq 19}$	-0.17	-1.13 to 0.78
$\sigma$	16.37	13.95 to 19.21	$\sigma$	3.17	1.25 to 8.06
			$d$	2.30	1.74 to 3.03

(a) Gaussian kernel (2).

(b) Lomax kernel (3)

Table 2: Estimated type-specific reproduction numbers with 95% confidence intervals based on parametric bootstrapping (199 samples from the asymptotic multivariate normal distribution of the parameters).

	Estimate	95% CI		Estimate	95% CI
B	0.22	0.17 to 0.31	B	0.26	0.14 to 0.35
C	0.10	0.06 to 0.15	C	0.13	0.06 to 0.19

(a) Gaussian kernel (2).

(b) Lomax kernel (3)

shows that also with the power-law kernel, the B-type is approximately twice as infectious as the C-type as measured by the  $\gamma_C$  parameter. However, the reproduction numbers become slightly larger for both types, which is related to the heavier tail of the power law enabling additional interaction between events at far distances.

We close this application with two additional ideas for improvement of the model. First, it might be worth considering a population effect also in the *epidemic* component to reflect higher contact rates and thus infectivity in regions with a denser population. Using the log-population density of the infective's district,  $\log \rho_{[t_j][s_j]}$ , the corresponding parameter is estimated to be  $\hat{\gamma}_{\log(\rho)} = 0.21$  (95% CI: -0.06 to 0.49), i.e. individual infectivity scales with  $\rho^{0.21}$ , where

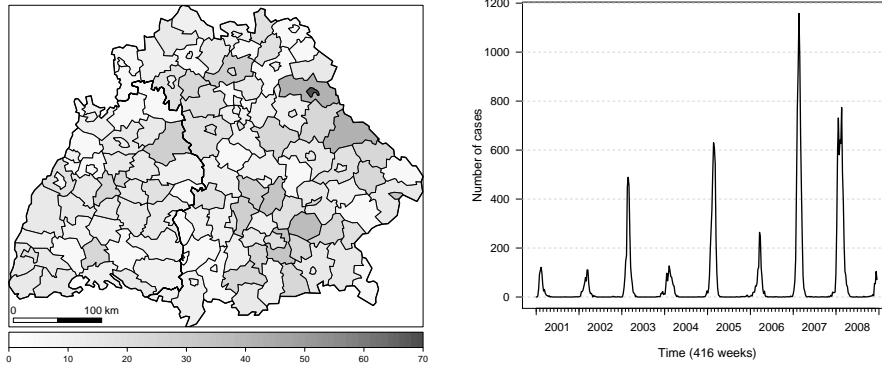


$\rho$  ranges from 39 to 4225 km<sup>2</sup>. Although the positive point estimate supports this idea, the wide confidence interval does not reflect strong evidence for such a population effect in the IMD data.

However, it is helpful to allow for spatial heterogeneity in the *endemic* component. For instance, an indicator for districts at the border or the distance of the district’s centroids from the border could serve as proxies for simple edge effects. The idea is that as we get closer to the edge of the observation window (Germany) more infections will originate from external sources not directly linked to the observed history of the epidemic within Germany. We thus model a spatially varying risk of importing cases through the endemic component. For the Greater Aachen Region in the central-west part of Germany, where a spatial disease cluster is apparent in Fig. 2a such a cross-border effect with the Netherlands was indeed identified by Elias et al. (2010) for the serogroup B finetype during our observation period using molecular sequence typing of bacterial strains in infected patients from both countries. Inclusion of an edge indicator improves AIC ( $\Delta\text{AIC} = -5$ ) with estimated rate ratio of 1.37 (95% CI: 1.10 to 1.70) for districts at the border versus inner districts. If we instead extend the endemic covariates  $\mathbf{z}_{[t][s]}$  of the power-law model by the distance to the border, AIC improves further ( $\Delta\text{AIC} = -20$ ) with an estimated risk reduction of 4.9% (95% CI: 2.9% to 6.9%) per 10 km increase in distance to the border.

## 4.2. Influenza surveillance data from Southern Germany (2001–2008)

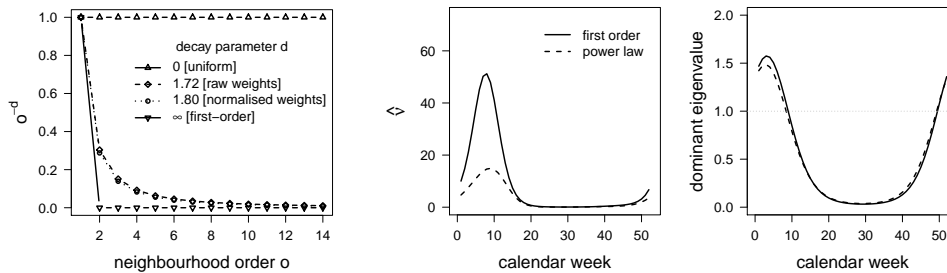
The best model (with respect to logS and RPS) for the influenza surveillance data found by Held and Paul (2012) using normalised first-order weights included  $S = 1$  sinusoidal wave in each of the autoregressive ( $\lambda_{it}$ ) and spatio-temporal ( $\phi_{it}$ ) components and  $S = 3$  harmonic waves with a linear trend in the endemic component  $\nu_{it}$  with the population fraction  $e_i$  in region  $i$  as offset. We now fit an extended model by estimating (raw or normalised) power-law neighbourhood weights (7) or (8) as described in Section 3.2, which replace the previously used fixed adjacency indicator.



(a) Mean yearly incidence per 100 000 inhabitants. (b) Weekly number of cases.

Figure 4: Spatial and temporal distribution of reported influenza cases in the 140 districts of Baden-Württemberg and Bavaria during the years 2001 to 2008.

Figure 5a shows the estimated power law, which is quiet similar for the normalised and raw formulations with  $\hat{d} = 1.80$  (95% CI: 1.61 to 2.01) and  $\hat{d} = 1.72$  (95% CI: 1.53 to 1.93), respectively. This decay is remarkably close to the power-law exponent 1.59 estimated by Brockmann et al. (2006) for short-time travel in the USA with respect to distance (in kilometres), even though neighbourhood order is a different and not even metric measure, and travel behaviour in the United States is potentially different from that in Southern Germany.



(a) Estimated power laws using raw (7) or normalised (8) weights. (b) Estimated seasonal variation using normalised weights. The plots for the raw weight models are very similar.

Figure 5: Estimated power laws (a) and seasonal variation (b).

Table 3: Estimated model parameters (with standard errors) excluding intercepts and trend/seasonal coefficients. The parameter  $\hat{\beta}_{1\log(\text{pop})}^{(\phi)}$  in the first row belongs to a further extended power-law model, which accounts for population in the spatio-temporal component (last column). The  $\sigma^2$  and  $\rho_{\cdot}$  parameters are the variances and correlations of the random intercepts (from  $\Sigma$ ). The last row shows the final values of the penalised and marginal log-likelihoods.

	raw weights		normalised weights		
	first order	power law	first order	power law	PL + pop.
$\hat{\beta}_{1\log(\text{pop})}^{(\phi)}$	—	—	—	—	0.76 (0.13)
$\hat{d}$	—	1.72 (0.10)	—	1.80 (0.10)	1.65 (0.10)
$\hat{\psi}$	0.93 (0.03)	0.86 (0.03)	0.92 (0.03)	0.86 (0.03)	0.86 (0.03)
$\hat{\sigma}_{\lambda}^2$	0.14	0.17	0.13	0.17	0.16
$\hat{\sigma}_{\phi}^2$	0.94	0.92	0.98	0.89	0.71
$\hat{\sigma}_{\nu}^2$	0.5	0.67	0.51	0.67	0.66
$\hat{\rho}_{\lambda\phi}$	0.02	0.2	0.03	0.21	0.13
$\hat{\rho}_{\lambda\nu}$	0.11	0.31	0.12	0.31	0.27
$\hat{\rho}_{\phi\nu}$	0.56	0.29	0.55	0.3	0.39
$l_{\text{pen}}(l_{\text{mar}})$	-18400 (-433)	-18129 (-456)	-18387 (-436)	-18124 (-453)	-18124 (-439)

Figure 5b shows the estimated seasonal variation in the endemic component, and the course of the dominant eigenvalue (Held and Paul, 2012) for the normalised weight models. The dominant eigenvalue is a combination of the two epidemic components: if it is smaller than 1, it can be interpreted as the epidemic proportion of total disease incidence, otherwise it indicates an outbreak period. Whereas the course of this combined measure is more or less unchanged upon accounting for higher-order neighbours with a power law, the weight of the endemic component decreases remarkably. This goes hand in hand with an increased importance of the spatio-temporal component since in the power-law formulation much more information can be borrowed from the number of cases in other regions. Jumps of the epidemic to non-adjacent regions within one week are no longer dedicated to the endemic component only.

Concerning the remaining coefficients, there is less overdispersion in the power-law models (see  $\hat{\psi}$  in Table 3), which indicates reduced residual heterogeneity. For the variance and correlation estimates of the random intercepts, there is no substantial difference between first-order and power-law models and even less between raw and normalised formulations.

To assess if the power-law formulation actually improves the previous first-

order model, predictive performance of the models is compared based on one-week-ahead predictions for all 140 regions and the 104 weeks of the last two years. Computing these predictions for one model takes about 3 hours (@2.80GHz using a single CPU), since the model needs to be refitted for every time point. Table 4 shows the resulting mean scores with associated  $p$ -values. Both logS and RPS improve when accounting for higher-order neighbours with a power law, while the difference is only significant for the logarithmic score. Furthermore, the normalised formulation performs slightly better than the raw weights. For instance, the mean difference in the logarithmic scores of the power-law models has an associated  $p$ -value of 0.0009. In the following, we therefore only consider the normalised versions. For additional comparison, the simple uniform weight model ( $w_{ji} \equiv 1$ ), which takes into account higher-order neighbours but with equal weight, has mean logS = 0.5484 and mean RPS = 0.4215, and thus performs worse than a power law decay.

Table 4: Mean scores of  $104 \times 140$  one-week-ahead predictions over the last two years, accompanied with  $p$ -values for comparing power-law and first-order weights obtained via permutation tests with 19999 random permutations. Note that the values obtained for normalised first-order weights are slightly different from the ones published by [Held and Paul \(2012\)](#) due to a correction of a recording error in the last week of the influenza data.

	raw weights		normalised weights	
	logS	RPS	logS	RPS
first order	0.5522	0.4205	0.5511	0.4194
power law	0.5453	0.4174	0.5448	0.4168
$p$ -value	0.00005	0.11	0.0001	0.19

Similar to the point process model, further improvement of the model’s description of human mobility can be achieved by accounting for the district-specific population also in the spatio-temporal component. The idea is that there tends to be more traffic to regional conurbations, i.e., districts with larger population, which are thus expected to import a bigger amount of cases from neighbouring regions. Note that inclusion of the log-population in  $\mathbf{z}_{it}^{(\phi)}$  affects susceptibility rather than infectivity as in the epidemic component of the point process model. The influenza data yield an estimated coefficient (SE) of

$\hat{\beta}_{\log(\text{pop})}^{(\phi)} = 0.76$  (95% CI: 0.50 to 1.01), which provides strong evidence for such an agglomeration effect. This result agrees quite well with the finding of [Bartlett \(1957\)](#), that the number of infectious imports scales with the square root of the population size. The variance of the random intercept  $b_i^{(\phi)}$  of the spatio-temporal component is slightly reduced from 0.89 to 0.71 reflecting a decrease in residual heterogeneity between districts. The decay parameter is estimated to be slightly smaller in the extended model ( $\hat{d} = 1.65$  (95% CI: 1.45 to 1.86)) and all other effects remain approximately unchanged (see [Table 3](#)). However, the predictive performance improves only minimally, e.g., the logarithmic score decreases from 0.5448 to 0.5447 ( $p = 0.66$ ). This small change could be related to the random intercepts  $b_i^{(\phi)}$ , which replace parts of the population effect if it is not included as a covariate. Indeed, there is substantial correlation ( $r_{\text{Pearson}} = 0.41$ ) between  $\log(\text{pop}_i)$  and  $b_i^{(\phi)}$  in the model without an explicit population effect in  $\phi_{it}$  (see [Supplement A](#) for a scatterplot).

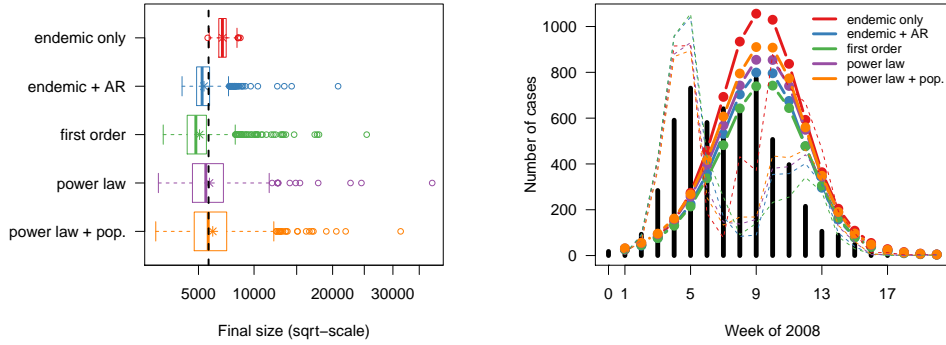
### 4.3. Long-term forecast of the 2008 influenza wave

For further evaluation of the power-law models described in [Section 4.2](#), we carry out a long-term forecast of the wave of influenza in 2008. Specifically, we simulate the evolution of the epidemic during the first 20 weeks in 2008 for each model trained by the previous years and initialised by the 18 cases of the last week of 2007 (see the animation in [Supplement A](#) for their spatial distribution). Predictive performance is then evaluated by the final size distributions and by proper scoring rules assessing the empirical distributions induced by the simulated counts both in the temporal and spatial domains. Since the logarithmic score is infinite in case of zero predictive probability for the observed count, we instead use the [Dawid and Sebastiani \(1999\)](#) score

$$\text{DSS}(P, y) = \frac{(y - \mu_P)^2}{\sigma_P^2} + \log \sigma_P^2,$$

where  $\mu_P$  and  $\sigma_P^2$  denote the mean and the variance of  $P$  (see also [Gneiting and Raftery, 2007](#)).

[Figure 6a](#) shows the final size distributions of the simulated waves of influenza



(a) Final size distributions ( $\sqrt{\cdot}$ -scale). The star in each box represents the mean, and the vertical dashed line marks the observed final size of 5781 cases. (b) Time series of observed (bars) and mean simulated (dots) counts aggregated over all districts. Week 0 corresponds to the initial condition (2007-W52). The dashed lines show the (scaled) RPS (see also Table 5).

Figure 6: Summary statistics of 1000 simulations of the wave of influenza during the first 20 weeks of 2008 for five competing models.

during the first 20 weeks of 2008. Note that model complexity increases from left to right and that we also considered the naive endemic model, i.e. independent counts, and the model without a spatio-temporal component as additional benchmarks. The endemic-only model, which only knows about region-specific intercepts, seasonality, and a log-linear time trend extrapolated from the counts of the previous years, overestimates the reported size of 5781 cases. It also does not allow for much variability in the size of the outbreak as opposed to the models with epidemic potential. The power-law models show the greatest amount of variation but best meet the reported final size: the power-law model without the population effect yields a simulated mean of 6022 (95% CI: 3126 to 10808). The huge uncertainty seems plausible with regard to the long forecast horizon over a whole epidemic wave.

Figure 6b shows the time series of observed and mean simulated counts aggregated over all districts. In 2008, the wave grew two or more weeks earlier than in previous years trained by the sinusoidal terms in the three components. This phenomenon cannot be captured by the simulations, which are solely based on the observed pattern during 2001-2007 and the distribution of the cases

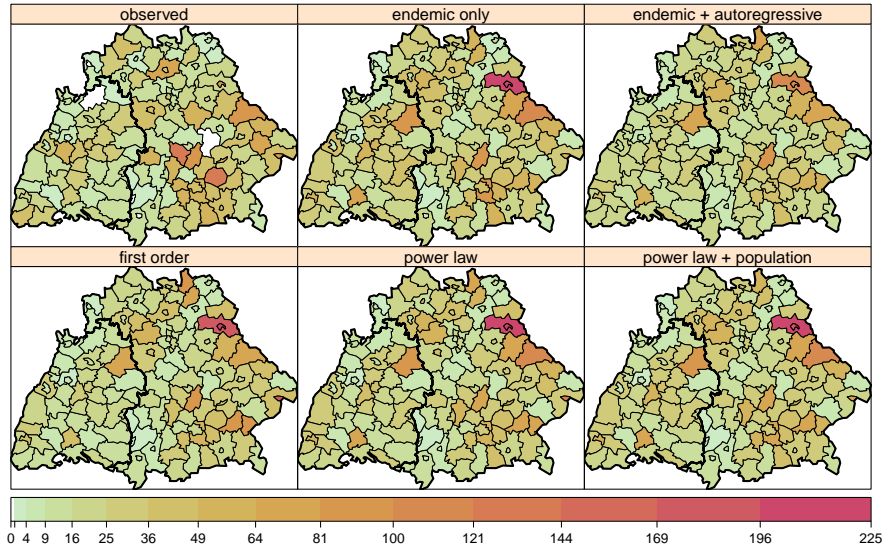


Figure 7: Observed and mean simulated incidence (cases per 100 000 inhabitants) aggregated over the 20 weeks forecast horizon (see Supplement A for scatterplots).

from the last week of 2007. Furthermore, instead of two peaks as observed specifically in 2008, the simulations yield a single, larger peak where the power-law models on average induce the best amplitudes with respect to final size. The simulated spatial distribution of the cases (see Fig. 7) is very similar among the various models and agrees quite well with the observed pattern. Animations of the observed and mean simulated epidemics provide more insight about the epidemic spread and are available as Supplement A. It is difficult to see a clear-cut traveling-wave of influenza in the reported data, which suggests that both an endemic component capturing immigration as well as scale-free jumps via the spatio-temporal component, i.e. power-law weights  $w_{ji}$ , are important. The animated series of weekly PIT histograms (using the non-randomised version for count data proposed by [Czado et al., 2009](#)) also included in the supplement mainly reflects the above time shift. More clearly than the plots, the mean scores in Table 5 show that predictive performance generally improves with increasing model complexity and use of a power law decay.

Table 5: Long-term predictive performance of 5 competing models in the temporal and spatial dimensions measured by mean DSS and RPS for the 2008 wave of influenza.

Model	Time		Space		Space-Time	
	DSS	RPS	DSS	RPS	DSS	RPS
endemic only	27.03	149.77	7.85	15.39	2.91	1.31
endemic + autoregressive	31.36	112.15	7.59	15.04	2.58	1.26
first order	26.46	108.61	7.51	15.63	2.50	1.26
power law	16.41	110.20	7.36	14.75	2.29	1.25
power law + population	15.49	111.86	7.24	14.30	2.29	1.24

## 5. Discussion

Motivated by the finding of [Brockmann et al. \(2006\)](#) that short-time human travel roughly follows a power law with respect to distance, we elaborated spatial power-law interaction in two modelling frameworks for spatio-temporal surveillance data. Since human mobility is an important driver of epidemic spread, the aim was to improve predictive performance of the models by replacing their naive Gaussian or first-order interaction formulations, respectively, by a more adequate description of human travel: a power law with respect to distance or neighbourhood order, respectively, where the decay parameter is estimated jointly with all other model parameters.

In both applications considered, the power-law formulations performed better. The most important feature of the power law is that it allows for long-range dependence between cases, which accordingly increased the epidemic weight in both models. An alternative formulation of spatial interaction with occasional long-range transmission was used by [Diggle \(2006\)](#), who added a small distance-independent value to a powered exponential term of the scaled distance. However, this offset and the power parameter were poorly identified so that the power was fixed at 0.5 for the 2001 UK foot-and-mouth disease epidemic to correspond to the transmission kernel estimated by [Keeling et al. \(2001\)](#).

Regions at the edge of the observation window are missing potential sources of infection from the unobserved side of the border. To capture unobserved heterogeneity due to immigration/edge effects, the count data model includes region-specific random intercepts  $b_i^{(v)}$  in the endemic component. However,



there was no clear pattern in their estimates with respect to regions being close to the border or not (Supplement A). In contrast, the IMD data supported edge effects, specifically concerning the border to the Netherlands. The spatial occurrence of cases met our simplistic approach of including the distance to the border as a covariate in the endemic component. This ignores that immigration might be more important in large metropolitan areas attracting people from abroad regardless of the location within Germany. A better way of accounting for edge effects would thus be to explicitly incorporate immigration data. For instance, [Geilhufe et al. \(2013\)](#) used incoming road or air traffic from outside North Norway as a proxy for the risk of importing cases of influenza, which led to improved predictive performance while also accounting for population in the spatio-temporal component.

Scaling regional susceptibility by population size proved very informative also for influenza in Southern Germany: More populated regions seem to attract more infections from neighbours than smaller regions, which reflects commuter-type imports (see [Viboud et al., 2006](#), and [Keeling and Rohani, 2008](#), Section 6.3.3.1). An exception of such a population effect in the spatio-temporal component might be seasonal accumulations in low-populated touristic regions. In the point process model for the IMD cases, the effect of population density on infectivity was less evident, which might be related to the very limited size of the point pattern with less than 100 cases per year over all of Germany.

We considered power laws as a description of spatial dispersal of infectious diseases as motivated by human travelling behaviour. Concerning temporal dispersal, power laws are usually not an appropriate description of the evolution of infectivity over time. Infectious diseases typically feature a very limited period of infectivity after the incubation period, since an infected individual will receive treatment and typically restrict its interaction radius upon the appearance of symptoms. Due to the small number of cases in the IMD data, we could not estimate a parametric temporal interaction function  $g(t)$  and simply assumed constant infectivity during 30 days. More generally,  $g(t)$  could represent an increasing level of infectivity beginning from exposure, followed by a plateau and then decreasing and eventually vanishing infectivity ([Lawson and Leimich, 2000](#), Section 5.3). Even simpler, the counts in the multivariate

time-series model were restricted to only explicitly depend on the previous week. This is reasonable if the generation time of the disease meets or at least is not larger than the time aggregation level in the surveillance data, which is true in our application: Human influenza was reported to have a mean generation time between 1 and 4 days, e.g., [Cowling et al. \(2009\)](#) report 3.6 days (95% CI: 2.9 days to 4.3 days).

The performed long-term forecast by simulation of the whole 2008 wave of influenza confirmed that the power-law model yields better predictions. However, the model was not able to detect an earlier onset of influenza than learned from the years 2001-2007. For this to work, it would be necessary to further enrich the model by external processes such as climate conditions entering as covariates in the endemic and/or epidemic components. Incorporation of vaccination coverage as in [Herzog et al. \(2011\)](#) could also improve the quality of predictions. Despite this deficiency, the simulated final size and spatial distribution matched the reported epidemic quite well.

This success also indicates that under-reporting of influenza seems to be roughly consistent over time and space. For instance, the 4 districts which did not report any cases during the 2008 forecast period (SK Kempten, SK Memmingen, LK Kelheim and SK Aschaffenburg) only reported 1, 0, 20 and 4 cases in total during 2001-2007. Of course, we can only model what is effectively reported from the epidemic, which may also be affected by time-varying attention drawn to influenza in the media. Syndromic surveillance systems aim to unify various routinely collected data sources, e.g., web searches for outbreak detection and monitoring ([Josseran et al., 2006](#); [Hulth et al., 2009](#)), and may thereby provide a more realistic picture of influenza.

Prospective detection of outbreaks is also possible based on the count data model presented here. A statistic could be based on quantiles of the distribution of  $Y_{i,t+1} | \mathbf{Y}_{\cdot,t}$ , e.g., an alarm could be triggered if the actual observed counts at  $t + 1$  are above the 99% quantile, say. Note that by including seasonality in the model, a yearly wave at the beginning of the year would be “planned” and not necessarily considered a deviation from default behaviour.

Future work on the count data model will incorporate network data such as plane and train traffic in the neighbourhood weights  $w_{ji}$  and try to *estimate* the

functional form of their impact on epidemic coupling between regions (Keeling and Rohani, 2002). Similarly, since the choice of a power law is a strong yet well motivated assumption, we aim to estimate the neighbourhood weight function or spatial dispersal kernel semi-parametrically from surveillance data. This could confirm if the power-law distribution of short-time human travel roughly copies to the modelling of infectious disease spread.

Use of the presented model frameworks in other applications is promoted by an implementation in the R package **surveillance**.

## 6. Software

All calculations have been carried out in the statistical software environment R 3.0.1 (R Core Team, 2013). Both model frameworks and their power-law extensions presented in this paper are implemented in the R package **surveillance** (Höhle et al., 2013) as of version 1.6-0 available from the Comprehensive R Archive Network (CRAN.R-project.org). The two analysed datasets are included therein as `data("imdepi")` (courtesy of the German Reference Centre for Meningococci) and `data("fluBYBW")` (raw data obtained from the German national surveillance system operated by the Robert Koch Institute, 2009). The point process model (1) for individual point-referenced data can be fitted by the function `twinstim()`, and the multivariate time-series model (5) for count data is estimated by `hhh4()`. The implementations are flexible enough to allow for other parametric specifications of the spatial interaction function  $f$  and the weights  $w_{ji}$ , respectively. A related two-component epidemic model (Höhle, 2009), which is designed for time-continuous individual surveillance data of a closed population with a fixed set of locations, e.g. for farm- or household-based epidemics, is also included as function `twinSIR()`.

For numerical log-likelihood maximisation, we generally used the quasi-Newton algorithm available through the R function `nlminb()`, which is based on FORTRAN 77 routines by Gay (1981). However, the marginal log-likelihood of the variance parameters in the multivariate time-series model (5) was maximised using `optim()`'s implementation of the Nelder and Mead (1965) algorithm.

The spatial integrals in the point process likelihood have been evaluated

using the product Gauss cubature implemented in the R package **polyCub** 0.3-1 (Meyer, 2013). Maps have been produced using **sp** 1.0-11 (Pebesma and Bivand, 2005), animations using **animation** 2.2 (Xie, 2013).

## A. Inference details

### A.1. Point process model

For a point pattern  $\{(t_i, \mathbf{s}_i) : i = 1, \dots, n\}$ , observed during the period  $(0; T]$  in region  $\mathbf{W}$ , the log-likelihood of a point process model, characterised through its conditional intensity function  $\lambda(t, \mathbf{s})$  with parameter vector  $\boldsymbol{\theta}$ , is given by

$$l(\boldsymbol{\theta}) = \left[ \sum_{i=1}^n \log \lambda(t_i, \mathbf{s}_i) \right] - \int_0^T \int_{\mathbf{W}} \lambda(t, \mathbf{s}) dt d\mathbf{s}$$

(Daley and Vere-Jones, 2003).

To find the maximum likelihood estimate most efficiently, we make use of the analytical score function and an approximation of the expected Fisher information worked out by Meyer et al. (2012, Web Appendices A and B). Both require the first partial derivatives of the spatial interaction function  $f(x)$  with respect to its parameters, which for the power laws with  $\tilde{\sigma} = \log(\sigma)$  and  $\tilde{d} = \log(d)$  optimised on the log-scale are as follows:

$$\frac{\partial f(x)}{\partial \tilde{\sigma}} = -d\sigma(x + \sigma)^{-d-1} \quad \frac{\partial f(x)}{\partial \tilde{d}} = -\frac{\log((x + \sigma)^d)}{(x + \sigma)^d}$$

for the Lomax kernel (3), and

$$\frac{\partial f_L(x)}{\partial \tilde{\sigma}} = \begin{cases} 0 & , \text{ for } x < \sigma \\ d \left(\frac{\sigma}{x}\right)^d & , \text{ otherwise} \end{cases}$$

$$\frac{\partial f_L(x)}{\partial \tilde{d}} = \begin{cases} 0 & , \text{ for } x < \sigma \\ -\frac{\log((x/\sigma)^d)}{(x/\sigma)^d} & , \text{ otherwise} \end{cases}$$

for the lagged power law (4).

## A.2. Count data model

Penalised likelihood inference for the count data model (5) proceeds by repeating the following two steps until convergence (Paul and Held, 2011):

1. numerical maximisation of the high-dimensional penalised log-likelihood  $l_{\text{pen}}(\boldsymbol{\theta}, \psi, \mathbf{b}; \boldsymbol{\Sigma})$  of the regression parameters given  $\boldsymbol{\Sigma}$ , where the vector  $\boldsymbol{\theta} = (\boldsymbol{\alpha}^{(\lambda)}, \boldsymbol{\beta}^{(\lambda)}, \boldsymbol{\alpha}^{(\phi)}, \boldsymbol{\beta}^{(\phi)}, d, \boldsymbol{\alpha}^{(v)}, \boldsymbol{\beta}^{(v)})^\top$  covers all fixed effects.
2. numerical maximisation of the (approximate) marginal log-likelihood  $l_{\text{mar}}(\boldsymbol{\Sigma})$  of the covariance matrix  $\boldsymbol{\Sigma}$  of  $\mathbf{b}_i$ .

Supplied with the penalised score function and Fisher information matrix, we maximise  $l_{\text{pen}}(\boldsymbol{\theta}, \psi, \mathbf{b}; \boldsymbol{\Sigma})$  using `nllminb()`. However, we maximise  $l_{\text{mar}}(\boldsymbol{\Sigma})$  by the Nelder and Mead (1965) algorithm, which does not require gradient calculations. This turned out to be twice as fast and generally more robust than the previously used quasi-Newton algorithm, since there are only six parameters in  $\boldsymbol{\Sigma}$  and evaluation of the marginal score function and Fisher information is complex.

The decay parameter  $d$  of the weight function (7) or (8), respectively, enters the penalised log-likelihood

$$l_{\text{pen}}(\boldsymbol{\theta}, \psi, \mathbf{b}; \boldsymbol{\Sigma}) = \sum_{i=1}^I \left[ \sum_{t=2}^T \log f(y_{it}; \mu_{it}(\boldsymbol{\theta}, \mathbf{b}, \mathbf{y}_{t-1}), \psi) \right] + \log p(\mathbf{b}_i; \boldsymbol{\Sigma})$$

via the mean  $\mu_{it}$  of  $f$ , the probability mass function of the negative binomial distribution. The score function component of  $d$  is

$$s(d) = \sum_{i=1}^I \sum_{t=2}^T \left( \frac{y_{it}}{\mu_{it}} - \frac{\psi^{-1} + y_{it}}{\psi^{-1} + \mu_{it}} \right) \frac{\partial \mu_{it}}{\partial d}$$

where

$$\frac{\partial \mu_{it}}{\partial d} = \phi_{it} \sum_{j \neq i} \frac{\partial w_{ji}}{\partial d} y_{j,t-1}$$

only involves the spatio-temporal component of the model. In addition to the first derivative  $\partial w_{ji} / \partial d$  of the weight function, we also need its second derivative to compute the Fisher information matrix.

For the raw power-law weights (7), first and second derivatives are given by

$$\frac{\partial w_{ji}}{\partial d} = -o_{ji}^{-d} \log o_{ji} \quad \text{and} \quad \frac{\partial^2 w_{ji}}{\partial d^2} = o_{ji}^{-d} (\log o_{ji})^2.$$

For normalised power-law weights (8) we obtain

$$\begin{aligned} \frac{\partial w_{ji}}{\partial d} &= w_{ji}(d) \cdot \left[ -\log o_{ji} - Q_j^{(1)}(d) \right] \quad \text{and} \\ \frac{\partial^2 w_{ji}}{\partial d^2} &= w_{ji}(d) \cdot \left[ \left( -\log o_{ji} - Q_j^{(1)}(d) \right)^2 - Q_j^{(2)}(d) + \left( Q_j^{(1)}(d) \right)^2 \right], \end{aligned}$$

where

$$Q_j^{(k)}(d) = \frac{\sum_{i=1}^I o_{ji}^{-d} (-\log o_{ji})^k}{\sum_{i=1}^I o_{ji}^{-d}}$$

for  $k \in \{1, 2\}$ . Estimation of  $d$  on the log-scale ( $\tilde{d} = \log d$ ), is performed using

$$\frac{\partial w_{ji}}{\partial \tilde{d}} = \frac{\partial w_{ji}}{\partial d} \cdot d \quad \text{and} \quad \frac{\partial^2 w_{ji}}{\partial \tilde{d}^2} = \frac{\partial^2 w_{ji}}{\partial d^2} \cdot d^2 + \frac{\partial w_{ji}}{\partial d} \cdot d,$$

which is true for both power-law formulations.

## Acknowledgements

We thank Michaela Paul for technical support on the original count data model, as well as Johannes Elias and Ulrich Vogel from the German Reference Centre for Meningococci, University of Würzburg, for providing us with the IMD data. This work was presented at the Summer School on Topics in Space-Time Modeling and Inference at Aalborg University, which enabled fruitful discussions with its participants. The research is financially supported by the Swiss National Science Foundation (project 137919: *Statistical methods for spatio-temporal modelling and prediction of infectious diseases*).

## Supplementary material

### Supplement A: Animations and additional plots

A bundle containing additional plots and the following space-time animations referenced in Section 4:

- Evolution of the influenza and IMD epidemics
- Observed and simulated counts from various models for the influenza epidemic during the first 20 weeks of the year 2008
- Weekly mean PIT histograms corresponding to these simulations

This supplementary material is available from <http://www.biostat.uzh.ch/research/manuscripts.html>.

## References

- Albert, R. and Barabási, A.-L. (2002). Statistical mechanics of complex networks. *Reviews of Modern Physics*, 74:47–97.
- Bartlett, M. S. (1957). Measles periodicity and community size. *Journal of the Royal Statistical Society. Series A (Statistics in Society)*, 120(1):48–70.
- Brockmann, D., Hufnagel, L., and Geisel, T. (2006). The scaling laws of human travel. *Nature*, 439(7075):462–465.
- Chis Ster, I. and Ferguson, N. M. (2007). Transmission parameters of the 2001 foot and mouth epidemic in Great Britain. *PLoS ONE*, 2(6):e502.
- Cowling, B. J., Fang, V. J., Riley, S., Peiris, J. M. S., and Leung, G. M. (2009). Estimation of the serial interval of influenza. *Epidemiology*, 20(3):344–347.
- Czado, C., Gneiting, T., and Held, L. (2009). Predictive model assessment for count data. *Biometrics*, 65(4):1254–1261.
- Daley, D. J. and Vere-Jones, D. (2003). *An Introduction to the Theory of Point Processes*, volume I: Elementary Theory and Methods of *Probability and its Applications*. Springer-Verlag, New York, 2nd edition.

- Dawid, A. P. and Sebastiani, P. (1999). Coherent Dispersion Criteria for Optimal Experimental Design. *The Annals of Statistics*, 27(1):65–81.
- Deardon, R., Brooks, S., Grenfell, B., Keeling, M., Tildesley, M., Savill, N., Shaw, D., and Woolhouse, M. (2010). Inference for individual-level models of infectious diseases in large populations. *Statistica Sinica*, 20(1):239–261.
- Diggle, P. J. (2006). Spatio-temporal point processes, partial likelihood, foot and mouth disease. *Statistical Methods in Medical Research*, 15(4):325–336.
- Diggle, P. J. (2007). Spatio-Temporal Point Processes: Methods and Applications. In Finkenstädt, B., Held, L., and Isham, V., editors, *Statistical Methods for Spatio-Temporal Systems*, chapter 1, pages 1–45. Chapman & Hall/CRC, Boca Raton.
- Diggle, P. J., Kaimi, I., and Abellana, R. (2010). Partial-likelihood analysis of spatio-temporal point-process data. *Biometrics*, 66(2):347–354.
- Elias, J., Schouls, L. M., van de Pol, I., Keijzers, W. C., Martin, D. R., Glennie, A., Oster, P., Frosch, M., Vogel, U., and van der Ende, A. (2010). Vaccine preventability of meningococcal clone, Greater Aachen Region, Germany. *Emerging Infectious Diseases*, 16(3):465–472.
- Farrington, C. P., Andrews, N. J., Beale, A. D., and Catchpole, M. A. (1996). A statistical algorithm for the early detection of outbreaks of infectious disease. *Journal of the Royal Statistical Society. Series A (Statistics in Society)*, 159(3):547–563.
- Gay, D. M. (1981). Computing optimal locally constrained steps. *SIAM Journal on Scientific and Statistical Computing*, 2(2):186–197.
- Geilhufe, M., Held, L., Skrvøseth, S. O., Simonsen, G. S., and Godtliebsen, F. (2013). Power law approximations of movement network data for spatio-temporal prediction of infectious disease spread. Revised for Biometrical Journal.
- Gibson, G. J. (1997). Markov chain Monte Carlo methods for fitting spatiotemporal stochastic models in plant epidemiology. *Journal of the Royal Statistical Society. Series C (Applied Statistics)*, 46(2):215–233.
- Gneiting, T. and Raftery, A. E. (2007). Strictly proper scoring rules, prediction, and estimation. *Journal of the American Statistical Association*, 102(477):359–378.
- Gneiting, T. and Schlather, M. (2004). Stochastic models that separate fractal dimension and the hurst effect. *SIAM Review*, 46(2):269–282.



- Gutenberg, B. and Richter, C. F. (1944). Frequency of earthquakes in California. *Bulletin of the Seismological Society of America*, 34(4):185–188.
- Hawkes, A. G. (1971). Spectra of some self-exciting and mutually exciting point processes. *Biometrika*, 58(1):83–90.
- Held, L., Höhle, M., and Hofmann, M. (2005). A statistical framework for the analysis of multivariate infectious disease surveillance counts. *Statistical Modelling*, 5:187–199.
- Held, L. and Paul, M. (2012). Modeling seasonality in space-time infectious disease surveillance data. *Biometrical Journal*, 54(6):824–843.
- Herzog, S. A., Paul, M., and Held, L. (2011). Heterogeneity in vaccination coverage explains the size and occurrence of measles epidemics in German surveillance data. *Epidemiology and Infection*, 139:505–515.
- Hulth, A., Rydevik, G., and Linde, A. (2009). Web queries as a source for syndromic surveillance. *PLoS ONE*, 4(2):e4378.
- Höhle, M. (2009). Additive-multiplicative regression models for spatio-temporal epidemics. *Biometrical Journal*, 51(6):961–978.
- Höhle, M., Meyer, S., and Paul, M. (2013). *surveillance: Temporal and Spatio-Temporal Modeling and Monitoring of Epidemic Phenomena*. R package version 1.6-0.
- Höhle, M., Paul, M., and Held, L. (2009). Statistical approaches to the monitoring and surveillance of infectious diseases for veterinary public health. *Preventive Veterinary Medicine*, 91(1):2–10. Special Issue: GisVet 2007.
- Josseran, L., Nicolau, J., Caillère, N., Astagneau, P., and Brückner, G. (2006). Syndromic surveillance based on emergency department activity and crude mortality: two examples. *Eurosurveillance*, 11(12):225–229.
- Keeling, M. J. and Rohani, P. (2002). Estimating spatial coupling in epidemiological systems: a mechanistic approach. *Ecology Letters*, 5(1):20–29.
- Keeling, M. J. and Rohani, P. (2008). *Modeling Infectious Diseases in Humans and Animals*. Princeton University Press.
- Keeling, M. J., Woolhouse, M. E. J., Shaw, D. J., Matthews, L., Chase-Topping, M., Haydon, D. T., Cornell, S. J., Kappey, J., Wilesmith, J., and Grenfell, B. T.

- (2001). Dynamics of the 2001 UK foot and mouth epidemic: stochastic dispersal in a heterogeneous landscape. *Science*, 294(5543):813–817.
- Lawson, A. B. and Leimich, P. (2000). Approaches to the space-time modelling of infectious disease behaviour. *IMA Journal of Mathematics Applied in Medicine and Biology*, 17(1):1–13.
- Le Comber, S., Rossmo, D. K., Hassan, A., Fuller, D., and Beier, J. (2011). Geographic profiling as a novel spatial tool for targeting infectious disease control. *International Journal of Health Geographics*, 10:35.
- Liljeros, F., Edling, C. R., Amaral, L. A. N., Stanley, H. E., and Aberg, Y. (2001). The web of human sexual contacts. *Nature*, 411(6840):907–908.
- Lomax, K. S. (1954). Business failures: another example of the analysis of failure data. *Journal of the American Statistical Association*, 49(268):847–852.
- Meyer, S. (2013). *polyCub: Cubature over Polygonal Domains*. R package version 0.3-1.
- Meyer, S., Elias, J., and Höhle, M. (2012). A space-time conditional intensity model for invasive meningococcal disease occurrence. *Biometrics*, 68(2):607–616.
- Nelder, J. A. and Mead, R. (1965). A simplex method for function minimization. *The Computer Journal*, 7(4):308–313.
- Newman, M. E. J. (2005). Power laws, Pareto distributions and Zipf’s law. *Contemporary Physics*, 46(5):323–351.
- Noufaily, A., Enki, D. G., Farrington, P., Garthwaite, P., Andrews, N., and Charlett, A. (2013). An improved algorithm for outbreak detection in multiple surveillance systems. *Statistics in Medicine*, 32(7):1206–1222.
- Ogata, Y. (1998). Space-time point-process models for earthquake occurrences. *Annals of the Institute of Statistical Mathematics*, 50(2):379–402.
- Pareto, V. (1896). *Cours d’Économie Politique*, volume 1. F. Rouge, Lausanne.
- Paul, M. and Held, L. (2011). Predictive assessment of a non-linear random effects model for multivariate time series of infectious disease counts. *Statistics in Medicine*, 30(10):1118–1136.

- Paul, M., Held, L., and Toschke, A. (2008). Multivariate modelling of infectious disease surveillance data. *Statistics in Medicine*, 27:6250–6267.
- Pebesma, E. J. and Bivand, R. S. (2005). Classes and methods for spatial data in R. *R News*, 5(2):9–13.
- Pinto, C. M., Lopes, A. M., and Machado, J. T. (2012). A review of power laws in real life phenomena. *Communications in Nonlinear Science and Numerical Simulation*, 17(9):3558–3578.
- R Core Team (2013). *R: A Language and Environment for Statistical Computing*. R Foundation for Statistical Computing, Vienna, Austria.
- Robert Koch Institute (2009). SurvStat@RKI. <http://www3.rki.de/SurvStat/>.
- Rossmo, D. K. (2000). *Geographic Profiling*. CRC Press, Boca Raton.
- Schrödle, B., Held, L., and Rue, H. (2012). Assessing the impact of a movement network on the spatiotemporal spread of infectious diseases. *Biometrics*, 68(3):736–744.
- Sommariva, A. and Vianello, M. (2007). Product Gauss cubature over polygons based on Green’s integration formula. *Bit Numerical Mathematics*, 47(2):441–453.
- Soubeyrand, S., Held, L., Höhle, M., and Sache, I. (2008). Modelling the spread in space and time of an airborne plant disease. *Journal of the Royal Statistical Society. Series C (Applied Statistics)*, 57(3):253–272.
- Stein, M. L. (1999). *Interpolation of Spatial Data: Some Theory for Kriging*. Springer.
- Viboud, C., Bjørnstad, O. N., Smith, D. L., Simonsen, L., Miller, M. A., and Grenfell, B. T. (2006). Synchrony, waves, and spatial hierarchies in the spread of influenza. *Science*, 312(5772):447–451.
- Wei, W. and Held, L. (2013). Calibration tests for count data. Submitted to *Biometrics*.
- Xie, Y. (2013). `animation`: An R package for creating animations and demonstrating statistical methods. *Journal of Statistical Software*, 53(1):1–27.
- Zipf, G. K. (1949). *Human Behavior and the Principle of Least Effort: An Introduction to Human Ecology*. Addison-Wesley Press, Cambridge, Massachusetts, USA.